

Comparison of multi-microphone probes and estimation methods for pressure-based acoustic intensity

Michael T. Rose, Reese D. Rasband, Kent L. Gee, and Scott D. Sommerfeldt

Citation: *Proc. Mtgs. Acoust.* **26**, 030004 (2016); doi: 10.1121/2.0000787

View online: <https://doi.org/10.1121/2.0000787>

View Table of Contents: <http://asa.scitation.org/toc/pma/26/1>

Published by the [Acoustical Society of America](#)



171st Meeting of the Acoustical Society of America

Salt Lake City, Utah

23-27 May 2016

Engineering Acoustics: Paper 2pEA3

Comparison of multi-microphone probes and estimation methods for pressure-based acoustic intensity

Michael T. Rose, Reese D. Rasband, Kent L. Gee and Scott D. Sommerfeldt

Physics and Astronomy, Brigham Young University, Provo, Utah, 84602; rose.michael@byu.edu; r.rasband18@gmail.com; kentgee@byu.edu; scott.sommerfeldt@byu.edu

Acoustic intensity measurements made with multi-microphone probes traditionally use cross-spectral processing methods to estimate pressure and particle velocity. Bias errors become significant as the microphone separation becomes comparable with the acoustic wavelength. However, it has been shown that the phase and gradient estimator (PAGE) method increases probe bandwidth without modifying microphone spacing [Thomas et al. *J. Acoust. Soc. Am.* 137, 3366-3376 (2015)]. In this study, acoustic intensity is estimated by both the PAGE method and the traditional method across two three-dimensional (3D) intensity probes and three 2D intensity probes. Probe performance is compared in the far field of a broadband noise-radiating loudspeaker located in an anechoic chamber. The results show increased frequency bandwidth using the PAGE method across all probe designs. For 3D probes, intensity level errors were least with a spherical probe. For the 2D probes, the accuracy of intensity level and direction estimates increased with the separation distance of the microphones.



1. INTRODUCTION

Acoustic vector intensity \mathbf{I} has proven useful in many sound engineering and physical applications. It is part of several standardized methods^{1,2,3} to obtain radiated power. It is also used in noise source identification,^{1,4} for characterizing building insulation,^{5,6} and measuring sound emission from noise sources *in situ*.⁷

An estimate of \mathbf{I} can be made currently using one of three techniques: the p-u method, the traditional p-p method, and the Phase and Amplitude Gradient Estimator (PAGE) p-p method. Each of these techniques calculates \mathbf{I} as

$$\mathbf{I} = \frac{1}{2} \text{Re}\{p\mathbf{u}^*\}, \quad (1)$$

where p is the complex pressure at a given frequency and \mathbf{u}^* is the complex conjugate of the particle velocity at a given frequency. The p-u technique directly measures p and \mathbf{u} which requires an intensity probe⁸ that has a particle velocity sensor. In environments where significant non-acoustic temperature and velocity fluctuations occur, the p-u technique has been shown to be less robust than other techniques.^{9,10} In such cases, a more robust technique is the p-p method. The traditional¹¹ p-p method and the Phase and Amplitude Gradient Estimator (PAGE)¹² p-p method require multiple microphones separated by a small distance d that are used to obtain collocated estimates of pressure and particle velocity. Each microphone pair may have a different spacing d .

An \mathbf{I} bias error is any deviation in the intensity estimate from the actual intensity in the field due to estimation method errors or scattering. The traditional method has inherent estimation errors at frequencies well below the spatial Nyquist frequency f_N , where f_N is defined as the frequency at which $d = \lambda/2$, λ being a wavelength. It also makes linear estimations of nonlinear complex pressure gradients. Jacobsen¹³ showed that two microphones facing each other separated by one diameter of the diaphragm with a solid spacer counterbalances this effect. The PAGE method addresses both errors without a solid spacer. One error that affects both p-p methods is scattering. Wiederhold demonstrated that scattering becomes significant when the assumption $ka \ll 1$ does not hold.¹⁴ Here, k is the wavenumber and a is the characteristic dimension of each microphone or probe component (typically the diameter of the diaphragm).

This paper demonstrates that the frequency bandwidth of an intensity calculation can be extended simultaneously in the lower frequencies as well as beyond f_N . Low frequency bandwidth is extended by reducing phase mismatch and probe scattering bias errors with a large d . High frequency bandwidth is extended with the PAGE method intensity formulation which is accurate up to f_N and with phase unwrapping well beyond f_N .

2. INTENSITY ESTIMATION METHODS

A. TRADITIONAL NUMERICAL METHODS

The p-p method relies on Euler's equation to indirectly obtain particle velocity \mathbf{u} through a pressure gradient. Euler's equation can be expressed as

$$\rho_0 \frac{\partial \mathbf{u}}{\partial t} = -\nabla p, \quad (2)$$

where ρ_0 is ambient density and t is time. The traditional p-p method defines ∇p as

$$\nabla p \approx \frac{p_2 - p_1}{d}, \quad (3)$$

where p_1 and p_2 refer to the complex pressure seen by a pair of microphones and d refers to the distance separating them. In practice, Fahy¹⁵ and Pavic¹⁶ show that the traditional one-dimensional active intensity, I^{TRAD} , simplifies to

$$I^{\text{TRAD}} = \frac{1}{\rho_0 \omega d} Q_{12}(\omega), \quad (4)$$

where $Q_{12}(\omega)$ is the quad-spectrum.

B. PAGE NUMERICAL METHODS

Rather than using the finite sum and difference of the real and imaginary parts of p , the PAGE method uses the gradient of the amplitude and phase of p , ∇P and $\nabla \phi$, to estimate I .¹² With this in mind, p is conveniently defined in terms of its magnitude and phase as

$$p(\mathbf{r}) = P(\mathbf{r})e^{-j\phi(\mathbf{r})}. \quad (5)$$

Substituting this definition of p , Eq. 5, into Euler's equation, Eq. 2, and solving for \mathbf{u} results in

$$\mathbf{u}(\mathbf{r}) = \frac{j}{\rho_0 \omega} \nabla p = \frac{j}{\rho_0 \omega} [\nabla P(\mathbf{r}) - jP(\mathbf{r})\nabla \phi] e^{-j\phi(\mathbf{r})}. \quad (6)$$

The PAGE method expressions for p and \mathbf{u} , Eq. 5 and Eq. 6, are inspired by the work of Mann *et al*¹⁷ and Mann and Tichy.^{18,19} Active intensity by the PAGE method is analytically expressed as

$$I^{\text{PAGE}} = \frac{1}{2\rho_0 \omega} P^2 \nabla \phi. \quad (7)$$

This formulation of active intensity is advantageous because it is accurate up to f_N and allows for phase unwrapping to extend beyond f_N .

A quick explanation how $\nabla \phi$ is calculated makes Eq. 7 more clear: The first-order estimate of $\nabla \phi$ is

$$\nabla \phi \approx (\mathbf{R}^T \mathbf{R})^{-1} \mathbf{R}^T \Delta \phi. \quad (8)$$

In Eq. 8, $\Delta \phi = -[\arg\{H_{12}\} | \dots | \arg\{H_{(N-1)N}\}]^T$ and $\mathbf{R} = [\mathbf{r}_2 - \mathbf{r}_1 | \dots | \mathbf{r}_N - \mathbf{r}_{N-1}]^T$ where H_{12} is a transfer function between two microphones and \mathbf{r} is the spatial vector from the center of the probe to an individual microphone. Microphone separation, \mathbf{d} , is then equal to $\mathbf{r}_2 - \mathbf{r}_1$.

3. EXPERIMENTAL SETUP

A. INTENSITY PROBES

This experiment determines an intensity probe geometry/processing method combination that has the least amount of bias error across the widest frequency bandwidth.

This experiment considers both two and three-dimensional (2D and 3D) intensity probes. The 3D probes are commercially-built G.R.A.S. intensity probes, whereas the 2D probes were designed and built in-house, with a microphone at each vertex of an equilateral triangle and an additional microphone at the center of the probe. For the 2D probe design, microphone spacing and size is varied to demonstrate how microphone spacing and size affects probe performance.

Figure 1 shows a photo of each probe. Probe A is the G.R.A.S. 3D Vector Probe Head Type 60LK. The microphones are $\frac{1}{4}$ " CCP Flush-Mounted Microphones Set Type 47LV embedded on the surface of a 30 mm diameter sphere in a regular tetrahedron geometry. Probe B is the G.R.A.S. 50VI-1 Vector intensity probe. It includes three pairs of $\frac{1}{2}$ " G.R.A.S. 40AI Sound-intensity microphones with a physical spacer $d = 2.5$ cm from the center of the probe to each microphone. The three variations on the 2D probe design are probe C with three $\frac{1}{4}$ " G.R.A.S. 40BD prepolarized pressure microphones spaced 1" from the center, probe D with the same three $\frac{1}{4}$ " microphones spaced 2" from the center, and probe E with three G.R.A.S. 46AE $\frac{1}{2}$ " CCP free-field phase matched microphones spaced two inches from the center. Each 2D probe includes an additional phase matched center microphone.

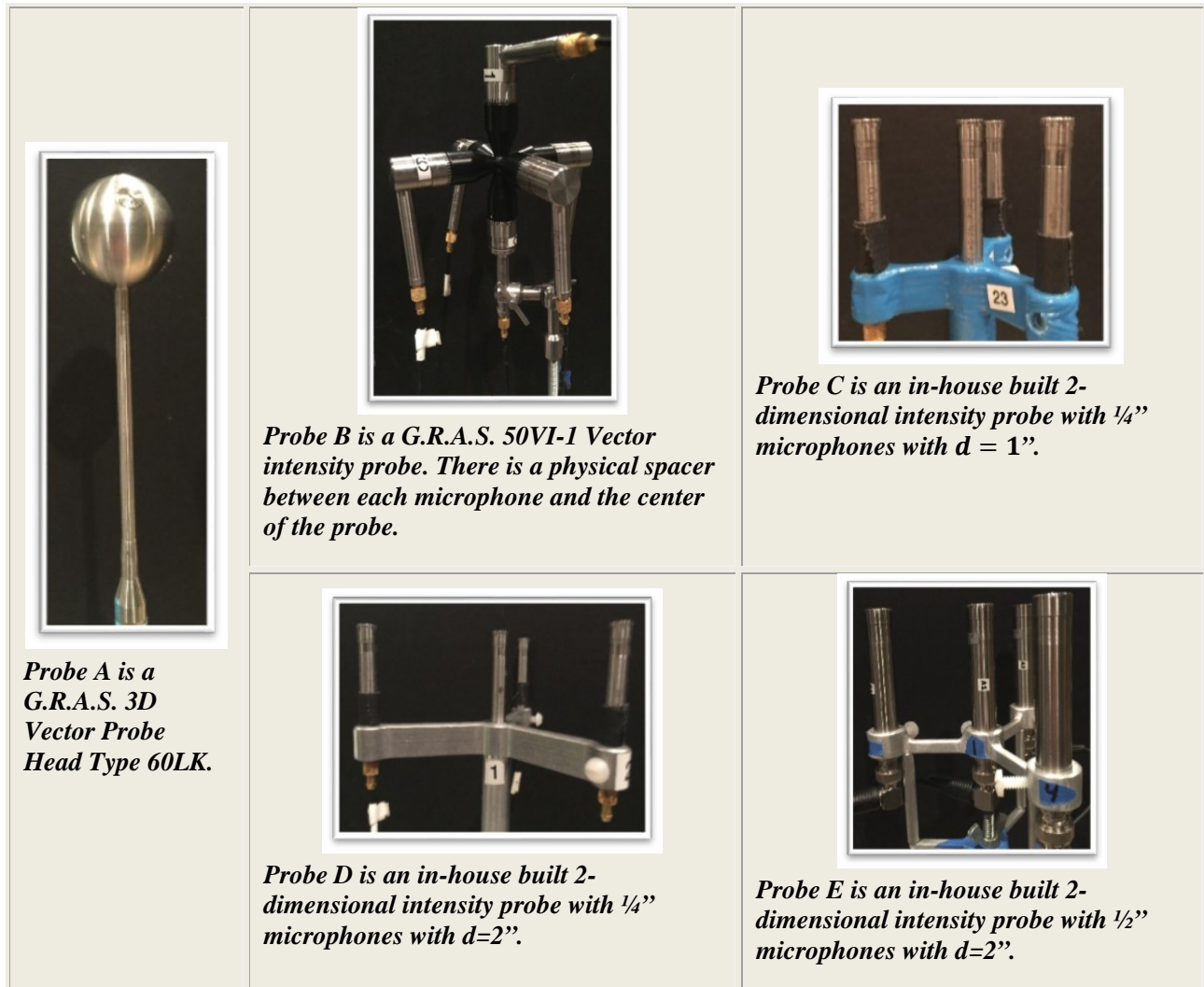


Figure 1: This figure contains a photo of each of the five intensity probes. Along with the photo is the probe's designation and description.

B. EXPERIMENT GEOMETRY

Each microphone probe was rotated 360° at 2.5° resolution since the angle of incidence of the impinging sound on the microphone probe was expected to cause different scattering patterns and other estimation errors. The experiment was performed in the BYU large anechoic chamber. A similar experiment was done by Giraud²⁰ and by Wiederhold.¹⁴ A Mackie HR624 studio monitor radiated broadband noise over its entire usable bandwidth of 47 Hz to 20 kHz. Each microphone probe was placed on a turntable 4.5

meters away from the Mackie speaker. Probes C and D were also placed 2 meters from the loudspeaker to verify SNR problems in the low frequencies.

The experimental setup allowed for a straightforward intensity level and direction benchmark. A single ¼ inch microphone was placed on the turntable to obtain the sound pressure level at that location (virtually equal to the intensity level under these circumstances). Also, the alignment of the probe relative to the loudspeaker provided a known intensity direction.

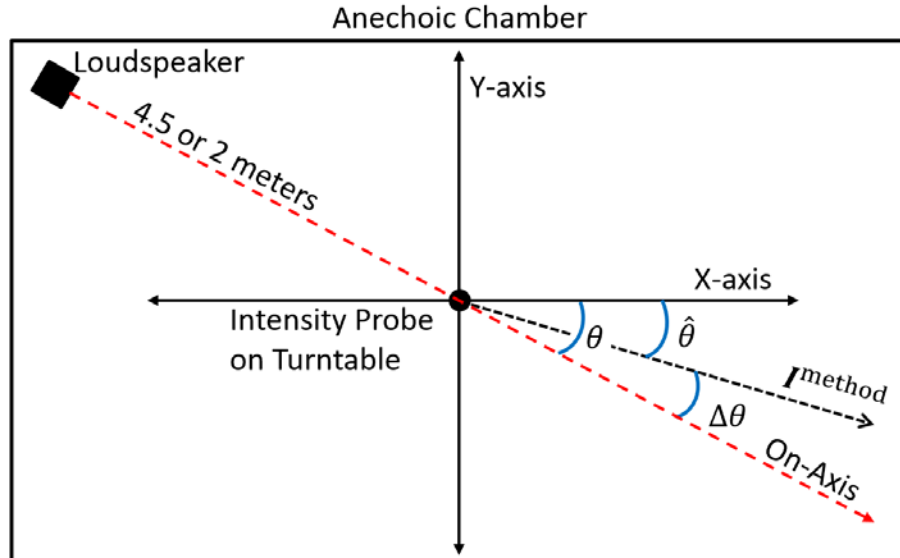


Figure 2: Schematic of the experimental setup. Three angles are shown. First, θ is the angle between the x-axis of the probe and the on-axis direction. Second, $\hat{\theta}$ is the angle between the estimated intensity direction and the probe's x-axis. Third, $\Delta\theta$ is the bias error angle of the estimated intensity direction relative to the known direction.

C. CALCULATING BIAS ERRORS

Intensity magnitude bias errors are the deviations in the estimated sound intensity level from the reference sound pressure level. This frequency-dependent error is calculated as

$$L_{I,err} = 10 \log_{10} \left| \frac{I^{\text{METHOD}}}{1 \text{pWm}^{-2}} \right| - 20 \log_{10} \left| \frac{p_{\text{rms,ref}}}{20 \mu\text{Pa}} \right| = L_I^{\text{METHOD}} - L_{p,\text{ref}}. \quad (9)$$

Intensity direction estimate errors are the deviations in the estimated intensity direction from the known orientation of the probe relative to the loudspeaker. This is calculated as

$$\Delta\theta = \theta - \hat{\theta}. \quad (10)$$

4. RESULTS AND DISCUSSION

Figures 3-7 describe the intensity magnitude and direction error of each microphone probe and processing method. Intensity magnitude errors in decibels calculated with Eq. 9 are displayed in plots “a” and “b” of each figure while intensity direction bias errors calculated with Eq. 10 are shown in plots “c” and “d” of each figure. The x-axis of each plot is frequency while the y-axis on each plot is the rotation angle θ , in degrees. Color corresponds to the bias errors calculated with the corresponding equation whether

magnitude or direction. In parts “a” and “b” in each figure, white represents $L_{I,err} = 0$ dB and in parts “c” and “d” white represents $\Delta\theta = 0^\circ$.

A. 3D PROBE RESULTS

Intensity estimate errors for probes A and B are shown in Figures 3 and 4 respectively. Probe A has low intensity magnitude bias error but has intensity direction bias errors dependent on θ . Probe A demonstrates minimal intensity magnitude error up to $f_N = 4.4$ kHz for the traditional method and through f_N to 20 kHz for the PAGE method. Probe A has undulations in intensity direction error for both methods, possibly due to spherical scattering. The traditional method limits the intensity direction to f_N while the PAGE method is only limited by the bandwidth being broadcast. The large low-frequency direction errors seen in Fig. 3b and 3d are due to the microphones’ high noise floor at low frequencies. The low SNR lowers the coherence between the microphones making the angle of the transfer function between microphones unreliable.

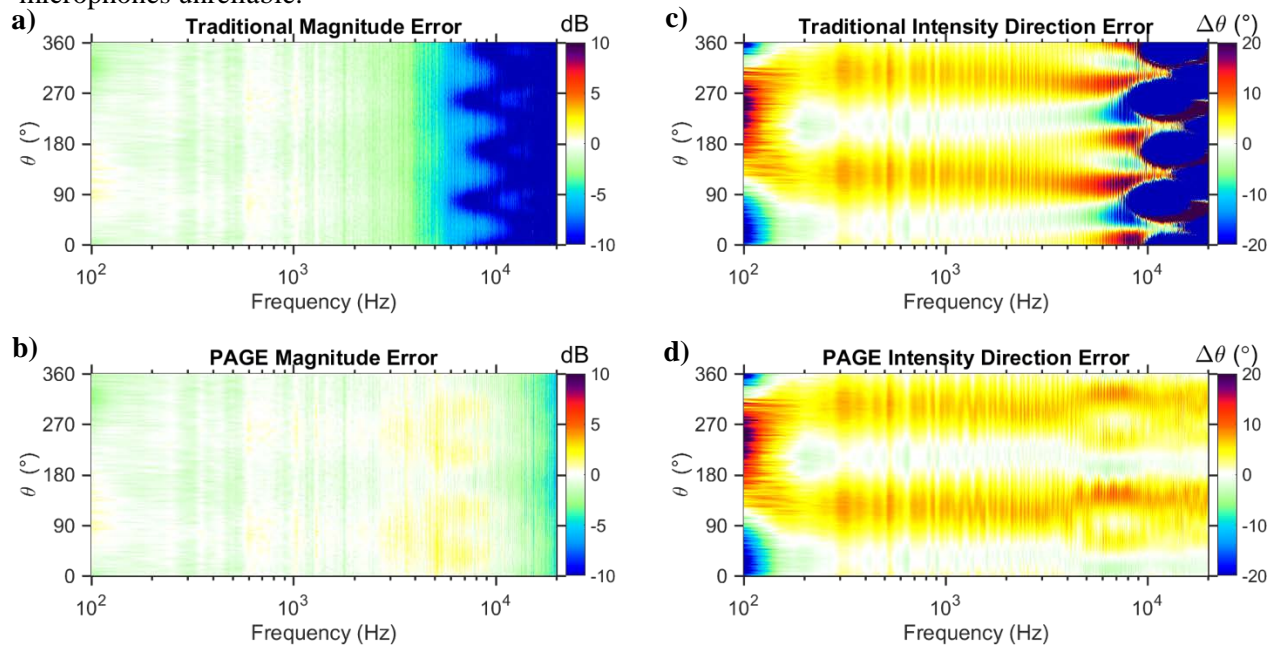


Figure 3. Probe A results display minimal intensity magnitude and direction errors. Direction errors are incident angle dependent. The PAGE method increases the usable frequency bandwidth. Parts a) and b) show intensity magnitude error in dB and parts c) and d) show intensity direction error in degrees. Parts a) and c) are processed using the Traditional method while parts b) and d) are processed using the PAGE method.

Probe B demonstrates large high frequency magnitude and direction error. Both the traditional and the PAGE method estimate intensity magnitude and direction up to $f_N = 3.4$ kHz. Frequencies higher than the spatial Nyquist frequency, f_N , are only obtainable through phase unwrapping and the PAGE method. Probe B has large physical spacers in between each microphone. These spacers scatter high frequencies causing intensity magnitude and direction bias errors above f_N . Jacobsen observed that diffraction effects from physical spacers compensate¹³ for the finite difference approximation error when microphones are positioned in the face-to-face arrangement. Jacobsen discovered that optimal compensation occurs when microphones are separated by a physical spacer the length of one microphone diameter. Unfortunately, the $\frac{1}{2}$ inch microphones of probe B are separated by spacers nearly two inches long causing its spatial Nyquist frequency to be relatively low. The spacers improve intensity magnitude estimates below f_N for the traditional method. Since the traditional (finite difference) method is band limited below f_N , high frequency scattering bias errors are washed out due to high frequency underestimation. Severe 3-5 dB scattering bias errors due to large physical spacers however, is apparent in Fig. 4b and 4d with the PAGE method for frequencies above f_N because the PAGE method does not underestimate high frequency intensity levels.

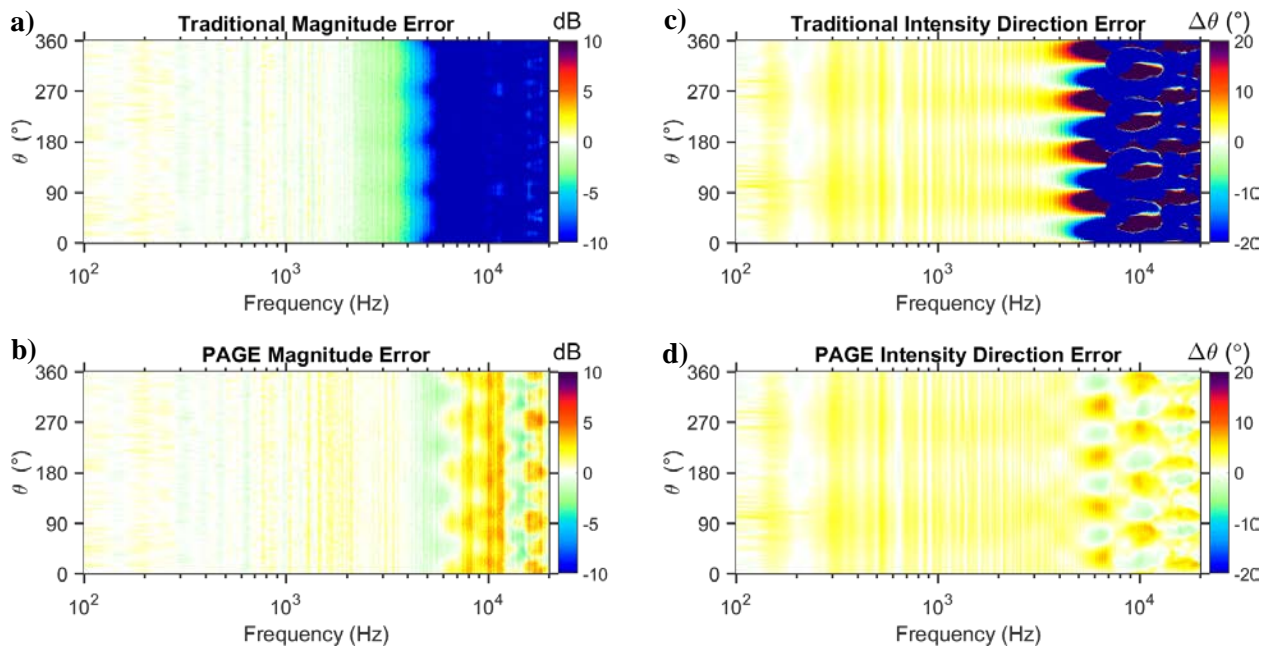


Figure 4. Probe B results display bias errors at frequencies above f_N due to scattering off large microphones and physical spacers. Parts a) and b) show intensity magnitude error in dB and parts c) and d) show intensity direction error in degrees. Parts a) and c) are processed using the Traditional method while parts b) and d) are processed using the PAGE method.

B. 2D PROBE RESULTS

Intensity estimate errors for probes C, D, and E are shown in Figures 5, 6, and 7 respectively. Probe C shows that for small d , 1 inch, phase mismatch error becomes large for low frequencies. The PAGE method also extends the probe bandwidth beyond $f_N = 3.9$ kHz up to the upper frequency broadcasted, 20 kHz.

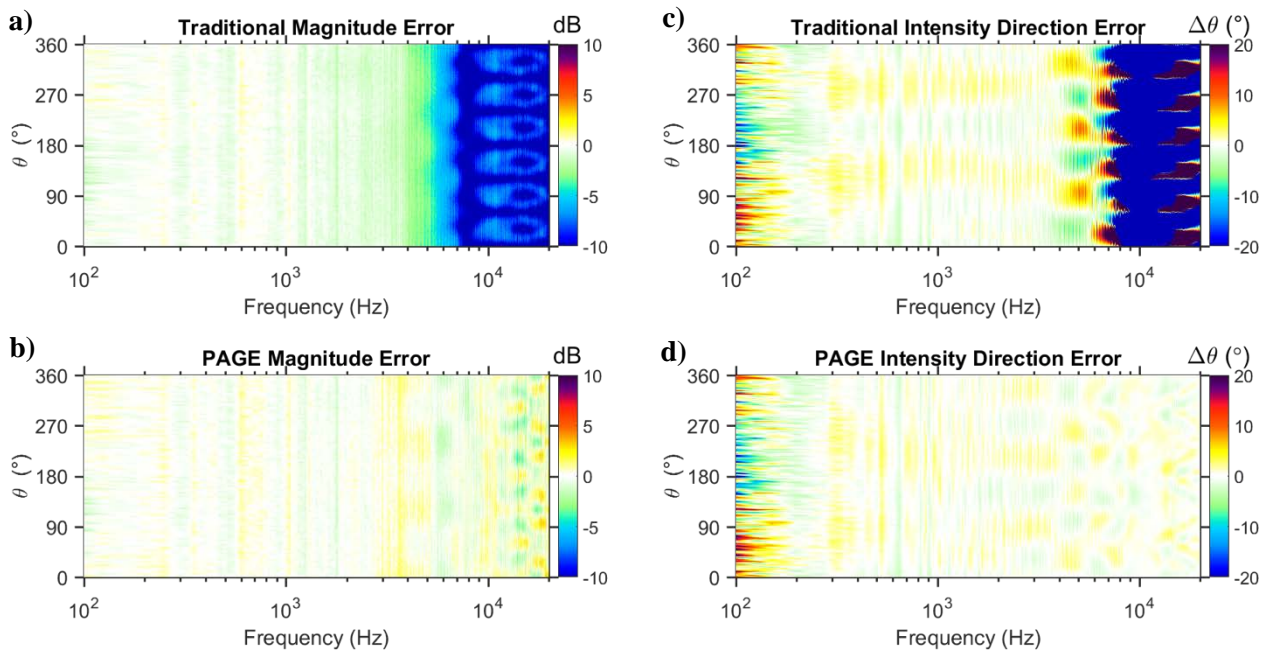


Figure 5. Probe C results display large bias errors at low frequencies due to significant phase mismatch compared to microphone spacing. Parts a) and b) show intensity magnitude error in dB and parts c) and d) show intensity direction error in degrees. Parts a) and c) are processed using the traditional method while parts b) and d) are processed using the PAGE method.

Probe D shows less phase mismatch error with a larger d , 2 inches. With the d being larger for probe D than probe C, it is expected with the traditional method that the probe's bandwidth be limited to a lower f_N . However, probe D does not lose high frequency magnitude or direction accuracy above $f_N = 1.9$ kHz as long as intensity is calculated with the PAGE method and phase unwrapped.

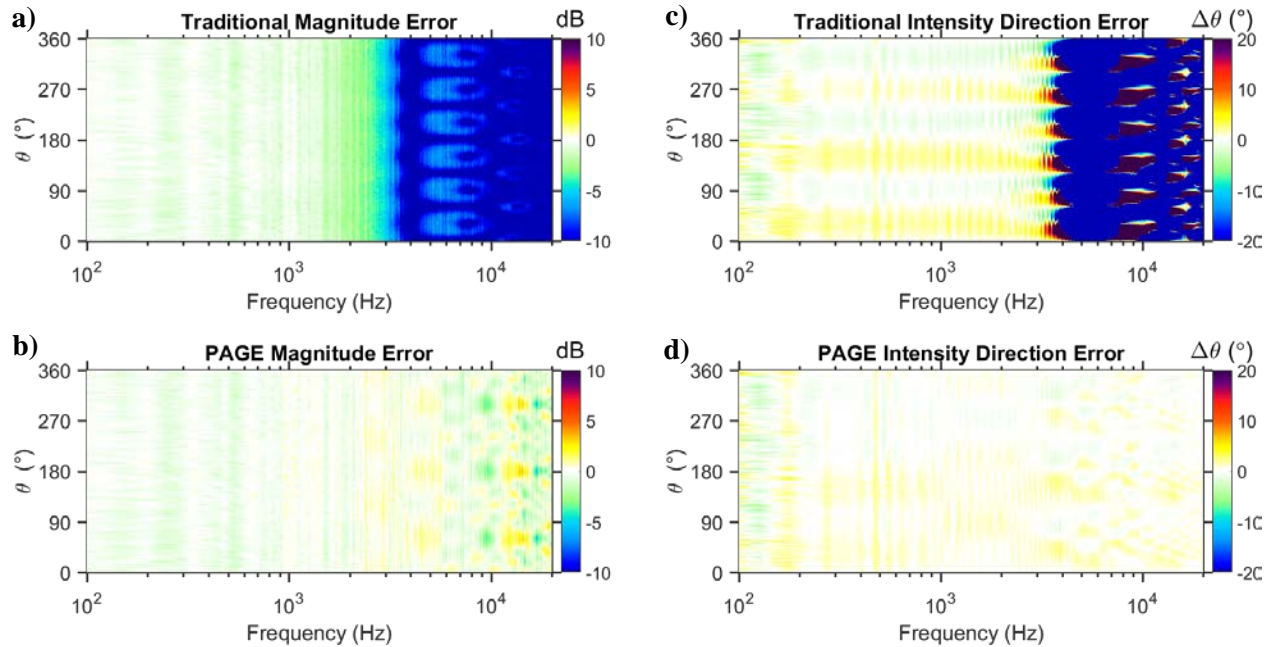


Figure 6. Probe D results display minimal low frequency bias errors due to a larger microphone spacing. High frequency scattering bias errors are low due to large microphone spacing and small microphone size. Parts a) and b) show intensity magnitude error in dB and parts c) and d) show intensity direction error in degrees. Parts a) and c) are processed using the Traditional method while parts b) and d) are processed using the PAGE method.

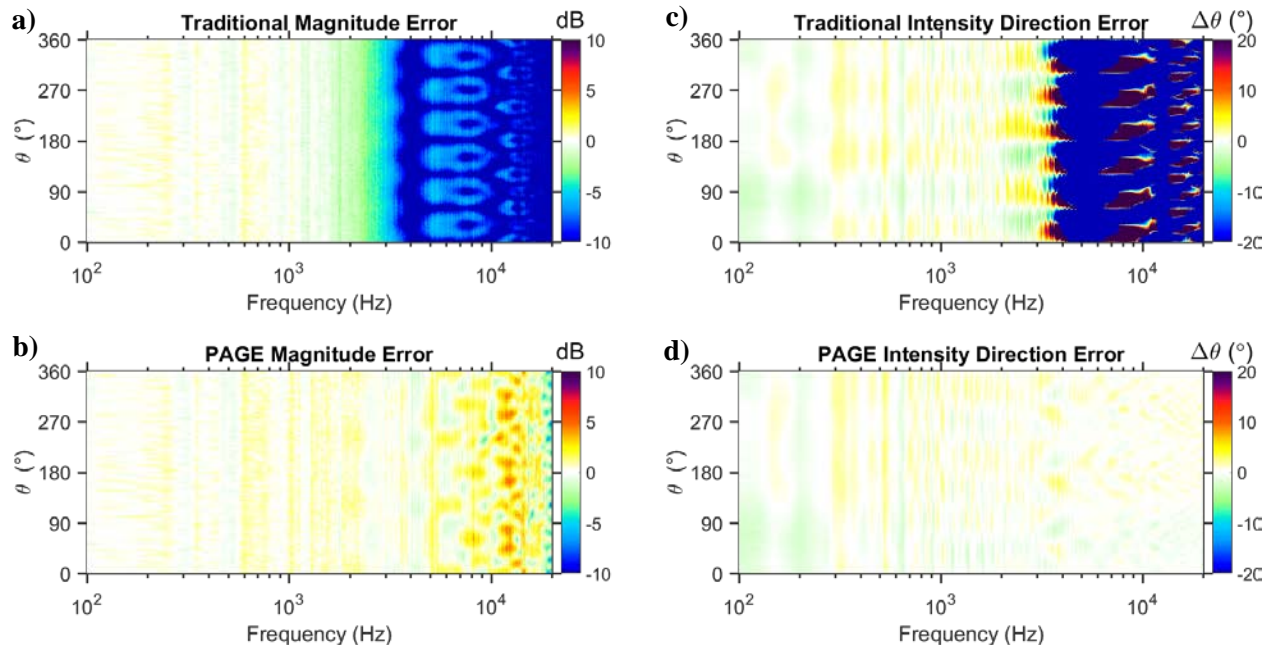


Figure 7. Probe E results display minimal low frequency bias errors due to better phase matching and large microphone spacing. Bias errors in the high frequencies are greater than probe D because probe E has larger microphones to cause more significant scattering.

Probe E shows more high-frequency scattering in the intensity magnitude bias error than probe D due to probe E's larger microphone size. Probe E has less low-frequency intensity direction bias error than probe C and D because the microphones used in probe E are phase matched to less than 0.1° .

5. CONCLUSION

The widest acoustic intensity frequency bandwidth estimation with the least bias error occurs when microphones are spaced far apart, smaller microphones are used, and the signals are processed with the PAGE method including phase unwrapping. Wider microphone separation reduces phase mismatch error. This is shown by the reduced phase mismatch error comparing probe D to probe C. Smaller microphone size and wider microphone separation reduces scattering. This is shown by the reduced high frequency magnitude bias errors of probe D as compared to probe C and E. The PAGE method allows for simultaneous high and low frequency bandwidth extension, even beyond the spatial Nyquist frequency with phase unwrapping for probes A-E and performs the best for probes that implement minimal scattering techniques (smaller microphones and larger inter-microphone spacing.)

ACKNOWLEDGMENTS

This work was supported by the National Science Foundation [Grant No. 1538550]. The authors acknowledge Tracianne Neilsen for helpful edits of an early draft of this manuscript.

REFERENCES

- ¹ T. Astrup, "Measurement of sound power using the acoustic intensity method — A consultant's viewpoint", *Appl. Acoust.*, 50(2), 111–123, (1997).
- ² ISO 9614-2:1996, "Acoustics—Determination of sound power levels of noise sources using sound intensity—Part 2: Measurement by scanning", International Organization for Standardization, (1996).
- ³ ISO 9614-3:2002, "Acoustics—Determination of sound power levels of noise sources using sound intensity—Part 3: Precision method for measurement by scanning", International Organization for Standardization, (2002).
- ⁴ S. Weyna, "The application of sound intensity technique in research on noise abatement in ships", *Appl. Acoust.*, 44(4), 341–351, (1995).
- ⁵ ISO 15186-1:2003, "Acoustics—Measurement of sound insulation in buildings and of building elements using sound intensity—Part 1: Laboratory measurements", International Organization for Standardization, (2003).

⁶ ISO 15186-2:2010, “Acoustics—Measurement of sound insulation in buildings and of building elements using sound intensity— Part 2: Field measurements”, International Organization for Standardization, (2003).

⁷ ISO 11205:2003, “Acoustics—Noise emitted by machinery and equipment—Engineering method for the determination of emission sound pressure levels in situ at the work station and at other specified positions using sound intensity”, International Organization for Standardization, (2003).

⁸ R. Raangs, W. F. Druyvesteyn, and H. E. De Bree, “A low-cost intensity probe,” *J. Audio Eng. Soc.* 51, 344–357 (2003).

⁹ F. Jacobsen, “Sound intensity measurements,” in *Handbook of Noise and Vibration Control*, edited by M. J. Crocker (Wiley, Hoboken, NJ, 2007), pp. 534–548.

¹⁰ J. H. Giraud, K. L. Gee, and J. E. Ellsworth, “Acoustic temperature measurement in a rocket noise field,” *J. Acoust. Soc. Am.* 127, EL179–EL184 (2010).

¹¹ F. Fahy, *Sound Intensity* (Spon, London, 2002), pp. 1–295.

¹² D. Thomas, B. Christensen, and K. Gee, “Phase and amplitude gradient method for the estimation of acoustic vector quantities,” *J. Acoust. Soc. Am.* 137, 3366–3376 (2015)

¹³ F. Jacobsen, V. Cutanda, and P. M. Juhl, “A numerical and experimental investigation of the performance of sound intensity probes at high frequencies,” *J. Acoust. Soc. Am.* 103, 953–961 (1998).

¹⁴ Wiederhold, C. P., Gee, K. L., Blotter, J. D., Sommerfeldt, S. D. and Giraud, J. H. (2014). “Comparison of multimicrophone probe design and processing methods in measuring acoustic intensity,” *The Journal of the Acoustical Society of America* 5, 2797-2807.

¹⁵ F. J. Fahy, “Measurement of acoustic intensity using the cross-spectral density of two microphone signals,” *J. Acoust. Soc. Am.* 62, 1057-1059 (1977).

¹⁶ G. Pavic, “Measurement of sound intensity,” *J. Sound Vib.* 51, 533–545 (1977).

¹⁷ J. A. Mann III, J. Tichy, and A. J. Romano, “Instantaneous and timeaveraged energy transfer in acoustic fields,” *J. Acoust. Soc. Am.* 82, 17–30 (1987).

¹⁸ J. A. Mann III and J. Tichy, “Acoustic intensity analysis: Distinguishing energy propagation and wave-front propagation,” *J. Acoust. Soc. Am.* 90, 20–25 (1991).

¹⁹ J. A. Mann III and J. Tichy, “Near-field identification of vibration sources, resonant cavities, and diffraction using acoustic intensity measurements,” *J. Acoust. Soc. Am.* 90, 720–729 (1991).

²⁰ J. Giraud, K. Gee, S. Sommerfeldt, T. Taylor, and J. Blotter, “Low-frequency calibration of a multidimensional acoustic intensity probe for application to rocket noise,” *Proceedings of Meetings on Acoustics*, Vol. 14, 2011.